



Core log integration: a hybrid intelligent data-driven solution to improve elastic parameter prediction

Zeeshan Tariq¹ · Mohamed Mahmoud¹ · Abdulazeez Abdulraheem¹

Received: 5 July 2018 / Accepted: 14 February 2019 / Published online: 26 February 2019
© Springer-Verlag London Ltd., part of Springer Nature 2019

Abstract

Current oil prices and global financial situations underline the need for the best engineering practices to recover remaining hydrocarbons. A good understanding of the elastic behavior of the reservoir rock is extremely imperative in avoiding the severe well drilling problems such as wellbore in-stability, differential sticking, kicks, and many more. Therefore, it is plausible to have a good estimation of the rock elastic behavior for successful well operations. This study presents a generalized empirical model to predict static Poisson's ratio of the carbonate rocks. Petrophysical well logs were used as inputs, and the laboratory measured static Poisson's ratio was used as an output. Three supervised artificial intelligence (AI) techniques were used, viz. artificial neural network (ANN), support vectors regression, and adaptive network-based fuzzy interference system. An extensive prediction comparison was made between these three AI techniques. Based on the lowest average absolute percentage error (AAPE) and highest coefficient of determination (R^2), the ANN model proposed to be the best model to predict static Poisson's ratio. To transform black box nature of AI model into a white box, ANN-based empirical correlation is also developed to predict the static Poisson's ratio. Comparison of the developed empirical correlation with previously established approaches to find static Poisson's ratio on an unseen published dataset revealed that the equation of ANN can predict the static Poisson's ratio with implicitly less AAPE and with high R^2 value. The proposed model with the empirical correlation can assist geo-mechanical engineers to predict the static Poisson's ratio in the absence of core data. The novelty of the new equation is that it can be used without the need of any AI software.

Keywords Static Poisson's ratio · Carbonate rocks · Triaxial tests · Well logs · Artificial intelligence · Particle swarm optimization · Mathematical model

Abbreviations

APE	Absolute percentage error
AAPE	Average absolute percentage error
ANFIS	Adaptive neuro-fuzzy inference system
ANN	Artificial neural network
CC	Correlation coefficient
FFNN	Feedforward neural network
LVDT	Linear variable differential transducer
MLP	Multilayer perceptron
PR	Poisson's ratio

RBF	Radial basis function
RMSE	Root mean square error
SVR	Support vectors regression
UCS	Unconfined compressive strength

List of symbols

b_1	Bias between input and hidden layer of neural network
b_2	Bias between hidden and output layer of neural network
c_1	Cognitive parameter ($0 \leq c_1 \leq 1.2$)
c_2	Cognitive parameter ($0 \leq c_2 \leq 1.2$)
E_{dyn}	Dynamic Young's modulus (MPsi)
E_{static}	Static Young's modulus (MPsi)
E_d	Dynamic Young's modulus (MPsi)
i	Index for neurons
j	Index for number of input parameters
n	Iteration number
N_h	Total number of neurons

✉ Zeeshan Tariq
g201406240@kfupm.edu.sa

Mohamed Mahmoud
mmahmoud@kfupm.edu.sa

Abdulazeez Abdulraheem
aazeez@kfupm.edu.sa

¹ Department of Petroleum Engineering, King Fahd University of Petroleum and Minerals, Dhahran 31261, Saudi Arabia

PR_{dyn}	Dynamic Poisson's ratio
PR_{static}	Static Poisson's ratio
P-wave	Compressional wave
p_i	Particle i position at any iteration
p_i^b	Particle best solution
p_{gb}	Global best solution
Rhob	Bulk density (g/cc)
R^2	Coefficient of determination
S-wave	Shear wave
w	Weight ($0 \leq w \leq 1.2$)
v_i	Weight ($0 \leq w \leq 1.2$)
w_1	Weights vector between input and hidden layer of neural network
w_2	Weights vector between hidden and output layer of neural network
x	Input parameters
y	Output variable
σ_o	Activation function between hidden and output layer of FFNN
σ_L	Activation function between input and hidden layer of FFNN
Δt_c	Compressional wave transit time ($\mu\text{s}/\text{ft}$)
Δt_s	S-wave transit time ($\mu\text{s}/\text{ft}$)
ρ	Bulk density (g/cc)
v_{dyn}	Dynamic Poisson's ratio

1 Introduction

Characterization of petroleum-bearing rocks needs a very high degree of accuracy. Minor error can lead to enormous loss of money and man-hours. On the contrary, a slight improvement in the prediction scenarios can have exponential improvement on production and exploration projects [1–5]. Current predictive models are fulfilling the basic needs of the petroleum industry, but there is an ever going quest for improved and better results [6]. AI tools once optimized for training can predict required feature more accurately than the nonlinear regression methods [7–10]. Some of the domains of the petroleum engineering in which AI techniques brought improvements include porosity–permeability predictions [11–14], hydraulic flow unit identification [15], geomechanics parameters estimation [16–22], geophysical well logs estimation [9, 23], well test parameters estimation [24, 25], asphaltene prediction [26, 27], water saturation prediction [28, 29], and many other oil and gas applications.

Elastic parameters are required to determine the in situ stresses of the rock which in turn are needed to construct the geo-mechanical earth models [30–34]. Determining elastic parameters of the rock is very substantial in minimizing the risk associated with the oil and gas well drilling.

Their accurate estimation helps in well placement optimization, calculating safe mud weight window, handling wellbore stability, optimizing fracturing operations, etc. [35–37]. These factors contribute to maximize the hydrocarbon recovery. Inaccurate estimation of the elastic parameters can falsely steer to wrong economic decisions and unsuitable field development strategies [9, 16, 38, 39].

Retrieving core samples and conducting laboratory experiments on them under a simulated reservoir condition is the accurate way to measure the in situ rock mechanical parameters, but this approach is very expensive as well as time-consuming [9, 17, 19, 40]. Often majority of the wells completed have very limited rock mechanical data. Alternatively, well log data are always recorded and readily available. Then, the correlations are developed between the elastic parameters obtained from the rock mechanical tests on the retrieved core sample and the available petrophysical well logs such as bulk density, neutron porosity, and sonic logs [41].

The correlations derived from the petrophysical logs are used to produce continuous static Poisson's ratio profile throughout the depth of interest [17, 30, 39]. However, core samples are taken from limited intervals, and the applicability of these correlations is mostly narrow [16, 38]. Often the calibration of dynamic Poisson's ratio profiles is carried out by computing the difference between the static Poisson's ratio and the dynamic Poisson's ratio of the selected core samples. This difference is added to the dynamic Poisson's ratio profiles to shift them near the points of static Poisson's ratio values [19, 40, 42]. This technique is very expensive and only limited to the sections where the core samples were obtained. Most important aspect of this relationship is that most of the time the scatter is too large to come up with a reasonable relationship and this relationship does not work for the entire interval in the case of lithology heterogeneity especially in carbonate reservoirs.

In the absence of the core data and other direct down-hole strength measurement, static Poisson's ratio is estimated from the well log data using empirical correlations. D'Andrea et al. [43] investigated the effect of ultrasonic wave transit time on static Poisson's ratio for different rock specimens and found that static Poisson's ratio decreases with the increase in transit time. Kumar et al. [44] applied nonlinear regression technique to predict static Poisson's ratio using P-wave and S-wave velocities. Phani [45] investigated the effect of shear wave velocity on static Poisson's ratio for materials with different pore size distributions. He found that materials containing needle-like and spherical shaped pores show that Poisson's ratio decreases with the decrease in S-wave velocity. Edimann et al. [46] and Kumar et al. [44] found that increase in porosity of the rock results in higher Poisson's ratio. They developed a correlation to predict static Poisson's ratio

using porosity. Al-Shayea [47] investigated the impact of micro-cracks and lithological variations on static Poisson's ratio values. He also correlated confining pressure with the static Poisson's ratio. Singh and Singh [48] used neuro-fuzzy approach to predict Poisson's ratio of sandstone and shale rocks. The input parameters of their model were uniaxial and triaxial strength parameters. Shalabi et al. [49] related static Poisson's ratio with rock hardness and unconfined compressive strength (UCS) using linear regression technique. Their correlation is valid for shale rocks only. Al-Anazi and Gates [50] used SVR to estimate static Poisson's ratio. The input variables of their SVR model were rock porosity, bulk density, pore pressure, minimum horizontal stress, overburden stress, P-wave velocity, and S-wave velocity.

With the reference of vast literature review and to the authors' knowledge, till now, no significant work has been done to formulate empirical correlation to estimate the static Poisson's ratio directly from petrophysical well logs for carbonate rocks. Most of the reported correlations in the literature were built using nonlinear regression technique which may not be generalized for unseen datasets [51]. On the down side, most of the AI models reported in the literature to predict static Poisson's ratio are black boxes [16, 50]. Therefore, the objectives of this study are to: (1) develop a generalized model using AI tools to predict the static Poisson's ratio from the commonly available conventional well logs such as bulk density, P-wave transit time, and S-wave transit time; (2) formulate tangible mathematical expression from the AI model to transform black box into white box to predict static Poisson's ratio of carbonate rocks.

2 Materials and methods

2.1 Log data analysis

Petrophysical well log data were taken from ten wells. The well logs data include neutron porosity, bulk density, P-wave transit time, and S-wave transit time. The petrophysical log data were picked from the reservoir depth where the cores were available for static tests. Lithology cross-plot of neutron porosity and bulk density shows that most of the samples lie in limestone formation with a low percentage of sandstone and dolomite and with no gas effects as shown in Fig. 1. The range of bulk density was in between 2.00 and 3.05 g/cc, P-wave transit time between 44 and 97 $\mu\text{s}/\text{ft}$, and S-wave transit time between 73 and 170 $\mu\text{s}/\text{ft}$. A complete statistical description of the data used for training is given in Table 1.

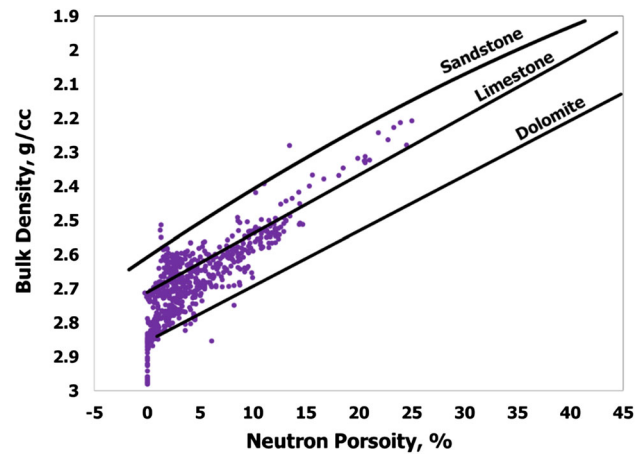


Fig. 1 Lithology cross-plot between neutron porosity and bulk density of the training data used for static Poisson's ratio model

2.2 Laboratory experiments

Core data were generated from the experiments performed using triaxial compressional tests. A total of 120 samples were tested to measure static Poisson's ratio. Extra care was taken to select homogeneous and sound samples free from any in situ cracks or weak stylolites. The dimensions of the prepared core samples were approximately 3" length and 1.5" diameter. The samples were prepared by cutting along the length of the reservoir core using a disk saw. The end faces of each core samples were carefully sliced and grounded parallelly to ensure fine smoothing. The fine smoothing is very essential; otherwise, it would have affected the experiment adversely by not allowing the pulse to transmit through the specimen because of air gap present in between crystal holder and specimen. To clean the core samples, toluene was used, and samples were then vacuum-dried in oven at 60 °C. Triaxial experiments were performed by placing the core sample axially while keeping a constant confining pressure corresponding to the effective in-situ horizontal stress. Each experiment was performed under dried and unsaturated condition. The samples were tested under room temperature, and confining pressures range from 1000 to 1500 psi. The samples were jacketed inside a heat-resistant rubber tubing. The rubber-jacketed core sample was then positioned between the steel end cap platens. Vacuum was used to remove any trapped air between steel end cap platens and jacketed sample. Using aluminum wires, the sample was then tightly secured with the end cap platens. After that, linear variable differential transducers (LVDTs) were mounted on the jacketed sample. The axial displacement was recorded using two LVDTs instrumented on the hardened steel platens opposite to each other with the help of an LVDT holder. The

Table 1 Training data statistics

Parameters	Max	Min	Mean	Range	SD	Skewness	Kurtosis
Bulk density, ρ (g/cc)	3.05	2.0	2.682	0.753	0.120	- 0.326	0.980
Compressional wave transit time, Δt_c (μ s/ft)	96.886	44.375	51.683	37.511	5.910	1.946	5.376
Shear wave transit time, Δt_s (μ s/ft)	170.496	73.187	95.922	73.309	10.089	1.190	3.491
Static Poisson's ratio	0.475	0.167	0.379	0.22	0.1186	- 0.533	0.829

radial displacement was measured using radial LVDT fixed at the center along the length of the sample.

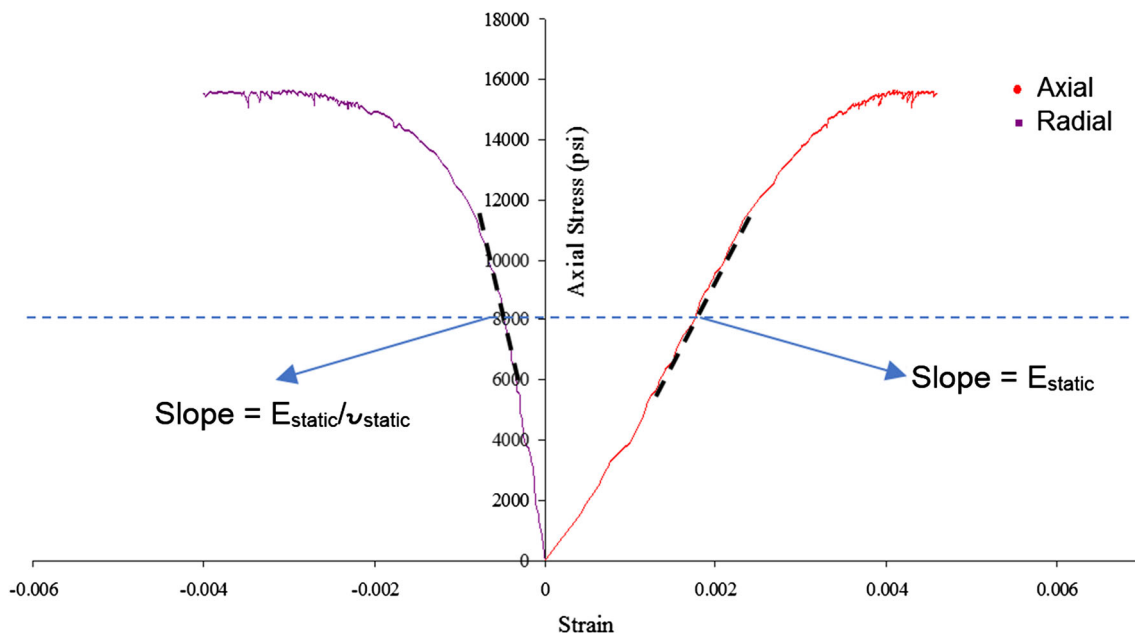
The confining pressure was increased to the required stage using desired rate in psi/sec by loading instrumented assembly in the confining chamber. The sample was loaded axially, after reaching the required value of confining pressure. The loading piston was lowered at a displacement rate of 0.025 mm/min. This displacement rate enabled the operator to complete the test according to the recommended practice of the American Society of Testing and Materials (ASTM D 2664-86, ASTM D 3148-93) and the International Society of Rock Mechanics (ISRM Suggested Methods, 13-127) [52]. During the loading phase, axial and radial displacements were recorded using LVDTs and the load on the sample was recorded using a load cell. Data acquisition was carried out using computer-controlled software. The stress–strain responses were generated for all samples, and elastic parameters (Poisson's ratio and Young's modulus) were calculated at 50% of the maximum peak stress. Figure 2 shows the stress–strain curve for one of the sample. A tangent line was drawn on axial stress–

strain curve (right side) at 50% of peak stress which is 8000 psi. The slope of this line yields static Young's modulus. On radial stress–strain curve (left side), another tangent line was drawn, and the slope of this line yields static Poisson's ratio. This procedure was repeated for all 120 samples.

2.3 Core and log data depth matching

Depth measured from well log values using wireline cables is usually not the same as the core depth, measured using drill strings. To remove any depth discrepancy, the first step taken was to match the log and the core depths. To achieve this, the petrophysical well log (neutron porosity) and laboratory measured values of core porosity were plotted together to visualize the difference between the log and the core depths. If there was any depth shift needed, then the correction was added or subtracted to the log depth, as given by Eq. (1)

$$\text{Depth}_{\text{Log}} = \text{Depth}_{\text{Core}} \pm \text{Depth}_{\text{Shift}} \quad (1)$$

**Fig. 2** Laboratory determination of static Poisson's ratio from the stress–strain curve

After that, depth column was removed to bring all the data on one set.

2.4 Correlation coefficient study

All AI models are data driven. The optimum way to select best input parameters is to find the relative importance by studying the correlation coefficient (CC) between inputs and the output parameter. The value of CC between the pair of two variables always lies in between -1 and 1 . A CC value close to -1 shows the strong inverse relationship between a pair of two variables, while a value close to 1 shows the strong direct relationship between the two variables. A CC value of zero shows that no relationship exists between the two variables. In this study, Pearson CC is used to find the relative importance between inputs and the static Poisson's ratio. The definition of Pearson CC is given in "Appendix A". Figure 3 shows the CC of P-wave transit time, S-wave transit time, bulk density, and neutron porosity with the static Poisson's ratio. P-wave transit time, S-wave transit time, and neutron porosity show an inverse relation with static Poisson's ratio, while bulk density shows a direct relation with static Poisson's ratio. P-wave transit time has the highest CC of -0.37 , while static Poisson's ratio, bulk density, and S-wave transit times have moderate CC of 0.35 and 0.29 with static Poisson's ratio. Neutron porosity has the lowest CC of -0.19 with the static Poisson's ratio. Due to the low CC of neutron porosity with the static Poisson's ratio, this input parameter was not used in the predictive modeling of static Poisson's ratio.

2.5 Data stratification

Dataset was divided randomly into two parts. 70% of the dataset was utilized for the training of the model, while the remaining 30% of the dataset was kept separate for the testing of the trained model. Data were stratified randomly

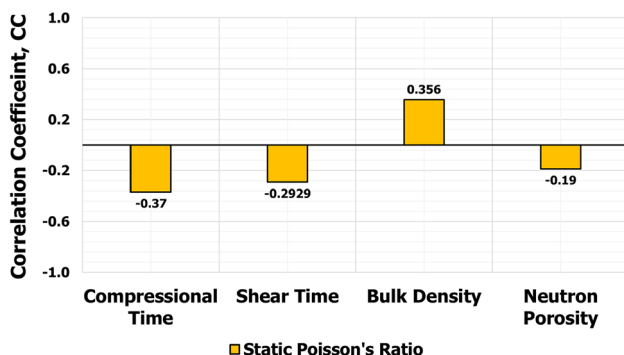


Fig. 3 Relative importance of the petrophysical well logs with the static Poisson's ratio

by the MATLAB in a way that the testing data bounded within the limits of the training dataset. This splitting process ensured that the testing data fall within the range of training data. Figure 4 shows the location of the data points for both the training and testing.

2.6 Design and implementation of the artificial intelligence techniques

2.6.1 Artificial neural network (ANN)

An ANN is a supervised data learning AI technique which is based on natural learning features of biological neurons found in human brain [54, 55]. ANN stands on the elemental information processing units called as neurons. Each neuron in the system is linked to a system of nodes, and the resulting structure looks like a biological neurons network [56]. Every connection has an associated weight [57, 58]. Several studies [39, 59, 60] suggested that back-propagation feedforward neural network is more robust than the multilayer perceptron (MLP). A typical ANN model comprises of an input layer, one or more hidden layers and an output layer. Signals are received by the input layer, transferred to the hidden layer(s) where they are processed, and then sent to the output layer. The hidden layer processes each dataset based on a transfer function. This function is based on different mathematical forms such as tan-sigmoid form expressed as $\sigma(x) = (2/1 + e^{-2x}) - 1$, the log-sigmoid form expressed as $\sigma(x) = 1/1 + e^{-x}$, or the linear function which is commonly implemented in multilayer networks trained by the backpropagation algorithm. Optimization of the number of layers and neurons is recommended since having too many neurons in the system can result in over-fitting or memorization problem. Having a fewer number of neurons in the system can result in under-fitting [53, 61].

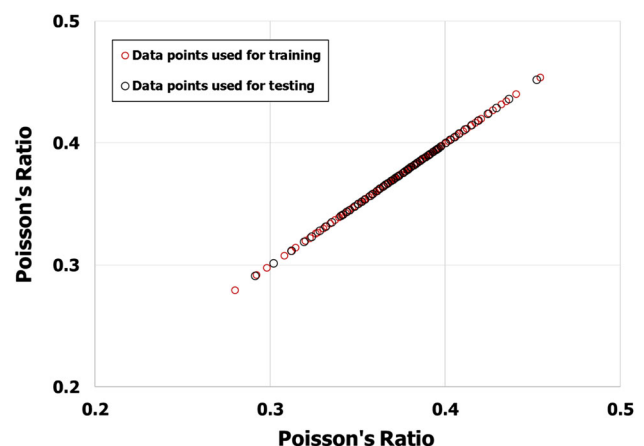


Fig. 4 Location of data points used for training and testing of the static Poisson's ratio models

2.6.2 Adaptive network-based fuzzy inference systems (ANFIS)

ANFIS is a supervised data learning technique, based on fuzzy logic to translate input data to the output by a combination of interconnected neural networks, initiated by Jang in 1993 [62]. It is a learning technique which uses Sugeno fuzzy inference system [62–64]. It is based on the application of conventional Boolean logic, i.e., zeros and ones, which describes the principle of truthiness [62, 64, 65]. The steps needed to apply for a typical ANFIS model are as follows: define inputs and an output variable; declare fuzzy sets; define fuzzy rules; create and train the network [66, 67]. In ANFIS, the important parameter is cluster radius which plays a vital role in the predictive performance. Cluster radius defines the number of if-then rules. Smaller value of cluster radius generates higher number of rules, while larger value of cluster radius generates smaller number of rules. In principle, higher number of rules causes the problems like overprediction and memorization [63].

2.6.3 Support vector regression (SVR)

SVR is a supervised learning technique that can be used for regression problems. SVR has a special feature of transforming a dataset into n-dimensional feature space by increasing the space of training examples in an optimum hyperplane [12, 68]. SVR’s performance relies on several factors that must be tuned properly to obtain an optimum predictive model. The use of SVR as related to oil and gas is both interesting and challenging because of scarcity of data as in geomechanics. It therefore becomes difficult to find enough dataset for training and testing of the model. The SVR has been used frequently in the past for the prediction of petroleum-related parameters [1–3, 26, 39, 69–74].

A linear regression-based function for SVR modeling can be expressed as Eq. (2)

$$f(\mathbf{x}) = \mathbf{w}^T \mathbf{x} + b \tag{2}$$

with input parameters $\mathbf{x}_k \in R^{N \times n}$ and output value $\mathbf{y}_k \in R^n$ for N given training points. The empirical risk factor is given by

$$R_{\text{emp}} = \frac{1}{N} \sum_{j=1}^N |y_k - \mathbf{w}^T \mathbf{x} - b|_{\varepsilon} \tag{3}$$

with Vapnik’s ε -insensitive loss function defined as

$$|y - f(\mathbf{x})|_{\varepsilon} = \begin{cases} 0, & |y - f(\mathbf{x})| \leq \varepsilon \\ |y - f(\mathbf{x})| - \varepsilon, & \text{otherwise} \end{cases} \tag{4}$$

This problem can be reformulated in dual space as

$$\begin{aligned} \max J_D(\alpha, \alpha^*) &= -\frac{1}{2} \sum_{j,l=1}^N (\alpha_k - \alpha_k^*) (\alpha_l - \alpha_l^*) \mathbf{x}_k^T \mathbf{x}_l \\ &\quad - \varepsilon \sum_{j=1}^N (\alpha_k + \alpha_k^*) + \sum_{j=1}^N y_k (\alpha_k - \alpha_k^*) \tag{5} \end{aligned}$$

subject to $\begin{cases} \sum_{k=1}^N (\alpha_k - \alpha_k^*) \\ \alpha_k, \alpha_k^* \in [0, c] \end{cases}$

where $\alpha_k, \alpha_k^* \geq 0$ are Lagrange multipliers.

Once the Lagrange multipliers are computed, the linear hypersurface regression function is given by Eq. (6)

$$f(\mathbf{x}) = \sum_{j=1}^N (\alpha_k - \alpha_k^*) \mathbf{x}_k^T \mathbf{x} + b \tag{6}$$

with

$$\mathbf{w} = \sum_{j=1}^N (\alpha_k - \alpha_k^*) \mathbf{x}_k \tag{7}$$

The training points with all nonzero values of α_k are assigned to the free support vectors, which allows the computation of the bias term b .

The nonlinear hyperplane regression equation can be given by Eq. 8

$$f(\mathbf{x}) = \sum_{j=1}^N (\alpha_k - \alpha_k^*) K(\mathbf{x}, \mathbf{x}_k) + b \tag{8}$$

where α_k, α_k^* are the solution of the quadratic programming problem in Eq. (8) and b is computed as a mean value for the free support vectors. The solution obtained will be unique and global if the kernel functions are positive and definite.

2.6.4 Particle swarm optimization (PSO)

Particle swarm optimization (PSO) is a computational technique that optimizes a given objective function by iterative method, originally applied by Kennedy and Eberhart [75]. A PSO technique is developed on the basis of inspiration earned from the social movements of various living organisms such as fish flocking and birds schooling [76, 77]. It is a stochastic optimization algorithm, computationally efficient and very simple to implement. PSO sets the best function evaluation particle as the global best and initializes each particle location as its local best. After initialization, PSO moves to the next iteration where by each particle in the swarm updates its velocity iteratively [78], using Eq. (9)

$$v_i(n+1) = wv_i(n) + \{c_1 \times \text{rand}[0, 1] \times (p_i^b - p_i(n))\} + \{c_2 \times \text{rand}[0, 1] \times (p_{\text{gb}} - p_i(n))\} \tag{9}$$

where w weight ($0 \leq w \leq 1.2$); v_i weight ($0 \leq w \leq 1.2$); c_1 cognitive parameter ($0 \leq c_1 \leq 1.2$); c_2 cognitive parameter ($0 \leq c_2 \leq 1.2$); n iteration number; p_i^b particle best solution; p_{gb} global best solution; p_i particle i position at any iteration.

The inertia term in the particle velocity equation ($wv_i(n)$) ensures that the particle moves toward its original direction, while its weight (w) ensures that the particle rate of acceleration moves toward its original direction. The cognitive component $c_1 \times \text{rand}[0, 1] \times (p_i^b - p_i(n))$ memorizes the particles' previous best solution. The social component $c_2 \times \text{rand}[0, 1] \times (p_{gb} - p_i(n))$ moves the particle toward the global best fitness. New position for each candidate solutions in the solution search space is generated by sum of the current position and velocity:

$$p_i(n + 1) = p_i(n) + v_i(n) \tag{10}$$

Objective function is evaluated to update the local best for each particle and then global best particle if the current best is better than the previous iteration. The whole process of velocity and particle position updating is repeated after objective function is evaluated to determine new improved quality solutions until a stopping criterion of maximum number of iteration is reached. Figure 5 summarizes the workflow adopted in this study to reach to the optimum model for the prediction of static Poisson's ratio. Steps related to the model testing and development of ANN equation are given in the next sections.

3 Prediction of static Poisson's ratio using artificial intelligence methods

A total of 120 data points were divided randomly into two sets with the proportion of 0.7:0.3. The set with 70% of the data (84 data points) was utilized for training of models, and the second set with 30% of the data (36 data points) was used to test the prediction competencies of trained models.

Three AI techniques, namely, ANN, ANFIS, and SVR, were implemented to develop models to predict static Poisson's ratio. A comparison was made between these three techniques based on the lowest AAPE and the highest R^2 between actual and predicted values. In ANN, two types of models were investigated, namely, feedforward neural network (FFNN) and radial basis function of neural network (RBF). In ANFIS too, two types of ANFIS models were studied, namely, Genfis-1 (Grid Partitioning) and Genfis-2 (Subtractive clustering). In SVR, two types of kernel functions were studied, namely, polynomial and Gaussian. Based on highest R^2 and lowest AAPE, FFNN,

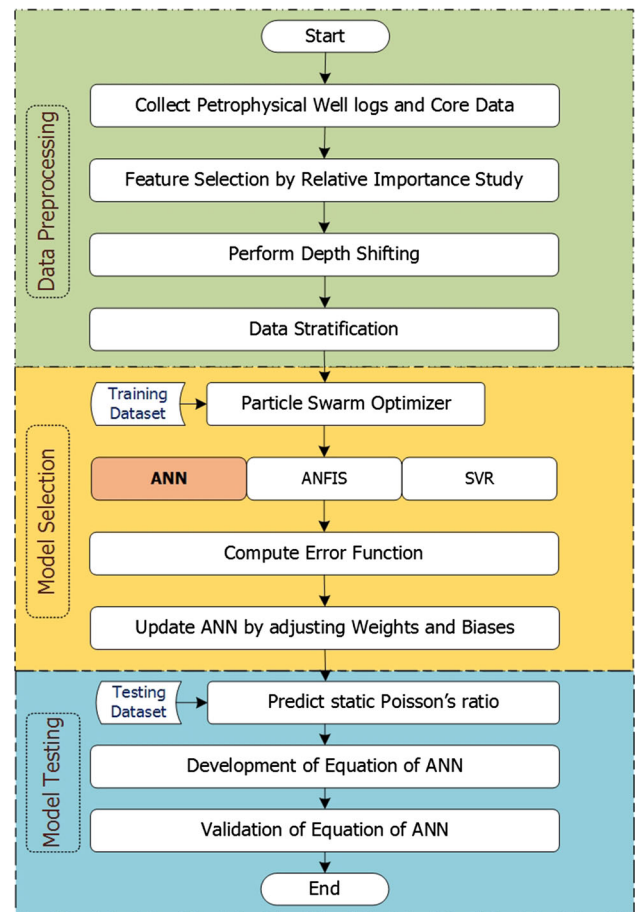


Fig. 5 Workflow of the proposed research study to model static Poisson's ratio

Genfis-2, and polynomial SVR were selected as best ANN, ANFIS, and SVR types to predict static Poisson's ratio.

For ANN, several runs were executed with various values of the model parameters. At every run, the parameters changed were learning rate, number of hidden layers with corresponding number of neurons, and different transfer functions. The SVR components of the model were tuned by optimizing several parameters, viz. kernel function, lambda, regularization parameters, epsilon, and kernel options. For ANFIS, in Genfis-2 the sensitivity of cluster radii was performed to reach the optimum model. The proposed model(s) were tuned by optimizing their several parameters by using particle swarm optimization. The complete list of AI techniques with optimizing parameters with their ranges is given in Table 2.

From PSO optimizer, optimized values of AI model parameters were obtained. The optimized FFNN model was based on three input layers, one hidden layer, and one output layer. In ANN, the optimum hidden layer number of neurons was found to be 20. Optimum transfer functions between input hidden layer were found to be tan-sigmoid,

Table 2 Summary of optimized parameters used for each technique in this study

AI techniques	Parameters	Ranges	Optimized values
Feedforward neural network (FFNN)	Number of inputs	3–4	3
	Number of hidden layers	1–3	1
	Number of output layers	1	1
	Number of neurons in the hidden layer	5–30	20
	Hidden layer transfer function	Tan-sigmoid, Log-Sigmoid, and Pure Linear	Tan-sigmoid
	Output layer transfer function	Pure Linear	Pure Linear
	Learning rate	0.01–0.9	0.12
	Network training algorithm	Levenberg–Marquardt, Bayesian Regularization, Resilient Backpropagation, Scaled Conjugate Gradient, Gradient Descent, Variable Learning Rate Gradient Descent, Polak-Ribière Conjugate Gradient, and BFGS Quasi-Newton	Levenberg–Marquardt
Adaptive network-based fuzzy inference system (ANFIS)	Type	Grid Partitioning and Subtractive Clustering	Subtractive clustering
	Value of radius	0.1–0.9	0.3
Support vectors regression (SVR)	Kernel function	Polynomial, Gaussian, and Radial Basis Function	Gaussian
	Kernel option	1.0–9.0	3.0
	Regularization parameter, C	500–5000	4500
	e-tube (epsilon)	0.01–0.05	0.05
	Lambda	1.0×10^{-1} – 1.0×10^{-5}	1.0×10^{-3}

and between hidden output layer found to be pure linear. Optimum learning algorithm found was backpropagation Levenberg–Marquardt with an optimum learning rate of 0.12. Hagan and Menhaj [79] also proved that the performance of FFNN with Levenberg–Marquardt learning algorithm is better than other learning algorithms in ANN. Figure 6 shows the architecture of the optimized FFNN model to predict static Poisson's ratio. The optimized Genfis-2 model was based on three input parameters and the one output parameter. Optimum cluster radius was found to have a value of 0.3. The optimized SVR model consists of three input parameters and one output parameter. Optimum kernel function was found to be the 'Gaussian' type with kernel options value of 3.0. Optimum value of regularization parameter was found to have a value of 4500. Optimum epsilon value found was 0.05 with an error tolerance of 1×10^{-3} . Multiple realizations were performed during the use of each AI technique to avoid them to get stuck at local minima.

On comparing the performance of all three models (ANN, ANFIS, and SVR), it was observed that during training, PSO-optimized ANN model yielded lowest AAPE and highest R^2 compared to PSO-optimized ANFIS and

SVR, as shown in Fig. 7. During the testing on unseen data, PSO-optimized ANN also outperformed PSO-optimized ANFIS and SVR by showing less AAPE and high R^2 values, as shown in Fig. 8. Table 3 lists the comparison of results for both training and testing of all three methods. Figure 9 shows the performance cross-plot by three models on overall data.

From the comparison analysis, it can be clearly observed that on the given set of the data, the developed ANN model was very generalized and can give good results on any unseen data within the range defined in Table 1. Therefore, ANN with three input parameters is suggested here as the best model for the prediction of static Poisson's ratio.

4 Development and validation of an equation of ANN

A FFNN model is created by a series of layers. Hidden layer neuron uses its weight w_1 , and bias b_1 , and its parameters are described by Eq. (11)

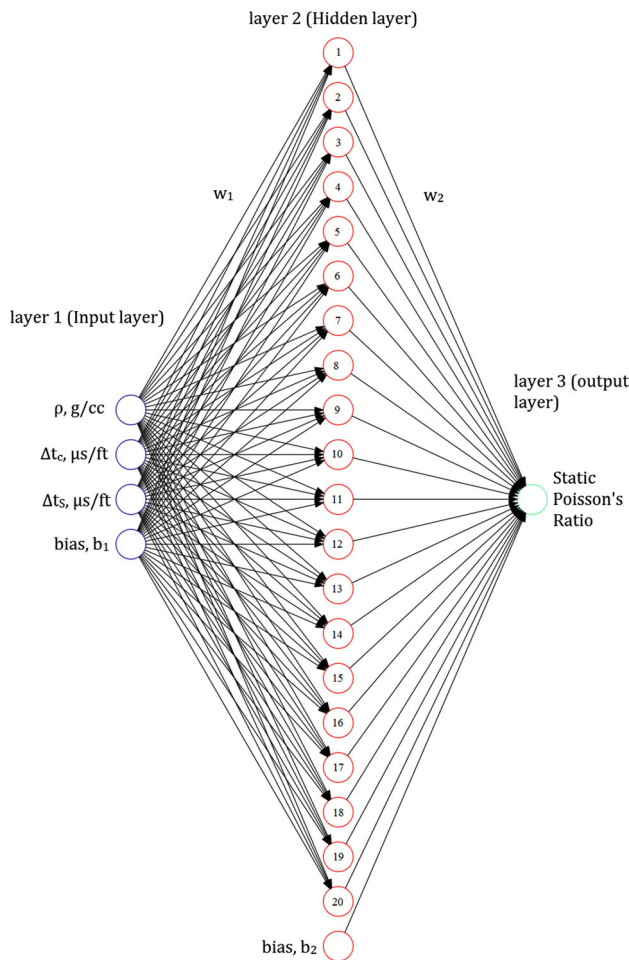


Fig. 6 Architecture of the trained FFNN model to predict static Poisson's ratio

$$\sigma_L \left(\sum_{j=1}^{N_p} w_{1,j} x_j + b_1 \right) \tag{11}$$

where N_p is the total number of inputs, x are the input parameters, and σ_L is the transfer function between the input and the hidden layer. The output of the whole network can be expressed as in Eq. (12):

$$\mu_P(\varphi) = \sigma_o \left[\sum_{i=1}^{N_h} w_{2,i} \sigma_L \left(\sum_{j=1}^{N_p} w_{1,i,j} x_j + b_{1,i} \right) + b_2 \right] \tag{12}$$

where N_h are the optimized number of neurons in the hidden layer, σ_o is the transfer function between the hidden layer and the output layer, and φ is a vector denoting the network parameters w_1, w_2, b_1 , and b_2 . In this study, ANN model is trained with three input variables ($\rho, \Delta t_C$, and Δt_S), with one hidden layer having twenty number of neurons, tan-sigmoid as an activation function between input and hidden layer, and pure linear as an activation function between hidden and output layer. Figure 10 shows

the architecture of the trained ANN for the prediction of static Poisson's ratio. An empirical expression is developed based on weights and biases of the trained ANN model. These extracted weights and biases are given in Table 4. Weights between the input layer and the hidden layer are a matrix which are referred as w_1 , and weights between the hidden layer and the output layer are a vector referred as w_2 . Biases between the input layer and the hidden layer are a vector referred as b_1 , and bias between the hidden layer and the output layer is a scalar referred as b_2 . The proposed equation of ANN of the static Poisson's ratio can be written more specifically as in Eq. (13)

$$PR_{static_n} = \sigma_o \left[\sum_{i=1}^{N_h} w_{2,i} \sigma_L (w_{1,i,1} \rho_n + w_{1,i,2} \Delta t_{C_n} + w_{1,i,3} \Delta t_{S_n} + b_{1,i}) + b_2 \right] \tag{13}$$

where $\sigma_L(x) = (2/1 + e^{-2x}) - 1, \sigma_o(x) = x$

The black box nature of ANN has been transformed into a white box by mining the weights and biases. This will allow the users of this paper to apply ANN-based mathematical model to predict static Poisson's ratio by simply plugging in the required input variables ($\rho, \Delta t_C$, and Δt_S) without the need of using AI software. Previously, artificial intelligence/machine learning-based models [80–86] were all black boxes in nature. In all these papers, authors mentioned only the approach they have used to train their models.

4.1 Procedure to use new equation of ANN for the prediction of static Poisson's ratio

The following three steps are required for using the new equation to predict static Poisson's ratio.

Step 1 Normalize input parameters ($\rho, \Delta t_C$, and Δt_S) between -1 and 1 . Input parameters are denoted here by 'x.' Normalization is needed to match the results from MATLAB ANN and equation of ANN. The difference of prediction from MATLAB ANN function and coding ANN (weights from MATLAB) is due to the normalization of input and output data. To get the same results with equation of ANN as from MATLAB ANN, normalization of input and output is required. The normalization of input is done by Eq. (14).

$$Input_{norm} = \frac{(Input_{max} - Input_{min})(x - x_{min})}{x_{max} - x_{min}} + Input_{min} \tag{14}$$

$Input_{min} = -1; Input_{max} = 1; x$ is the input parameter, x_{max} is the maximum value of the trained input parameter, and x_{min} is the minimum value of trained input parameter. x_{max} and x_{min} for each input parameters ($\rho, \Delta t_C$, and Δt_S)

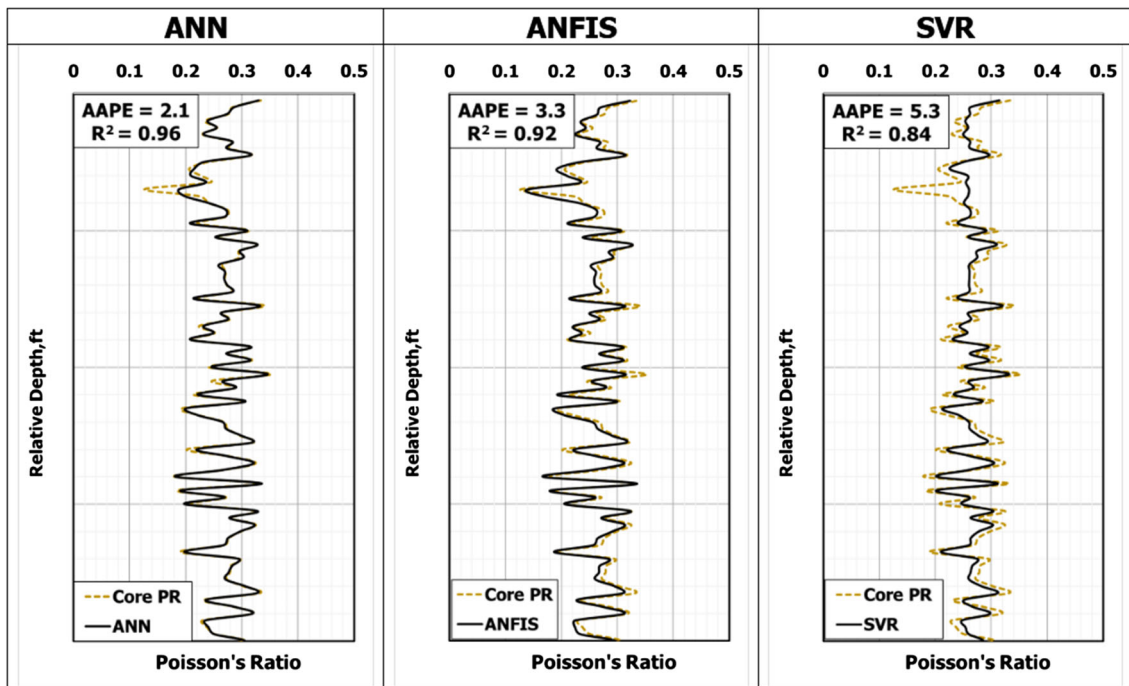


Fig. 7 Prediction of static Poisson’s ratio using three different AI techniques: ANN, ANFIS, and SVR (training comparison)

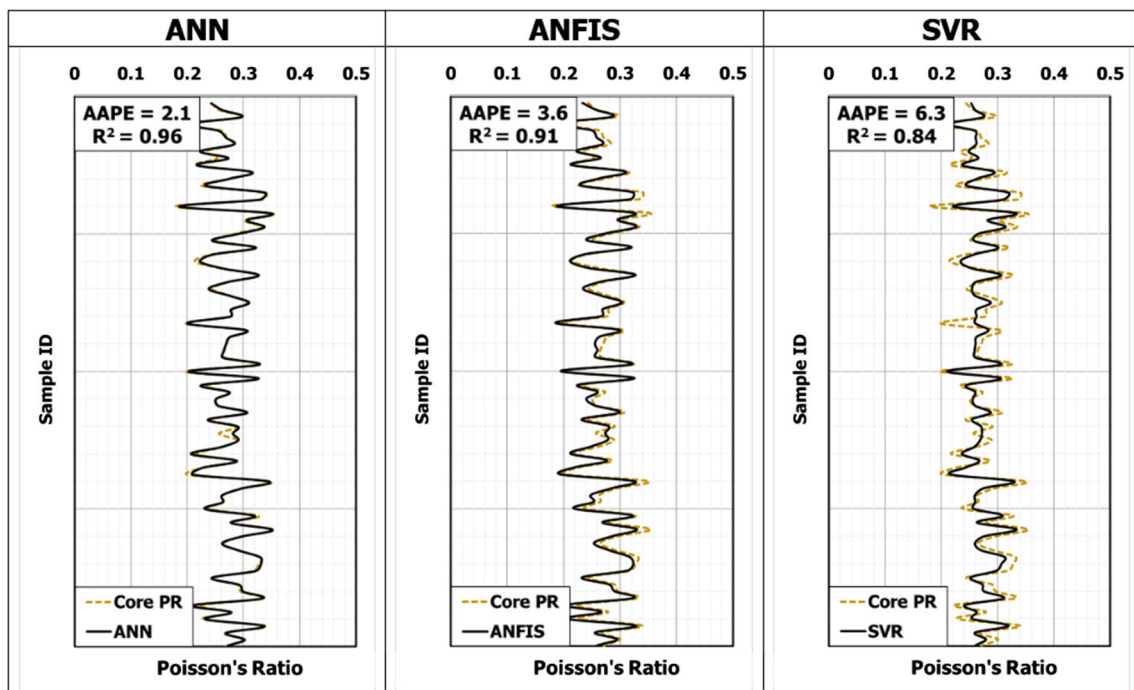


Fig. 8 Prediction of static Poisson’s ratio using three different AI techniques: ANN, ANFIS, and SVR (testing comparison)

are given in Table 1. To perform the normalization for $(\rho, \Delta t_C,$ and $\Delta t_S)$, Eqs. (15)–(17) can be used.

$$\rho_n = 2 \times \left(\frac{\rho - 2.01}{3.05 - 2.01} \right) - 1 \tag{15}$$

$$\Delta t_{C_n} = 2 \times \left(\frac{\Delta t_C - 44.375}{96.887 - 44.375} \right) - 1 \tag{16}$$

$$\Delta t_{S_n} = 2 \times \left(\frac{\Delta t_S - 73.187}{170.496 - 73.187} \right) - 1 \tag{17}$$

Table 3 Training and testing performances of AI methods

AI type	(70% Data) training set			(30% Data) testing set		
	AAPE	CC	R ²	AAPE	CC	R ²
Artificial neural network (ANN)	2.1	0.979	0.96	2.1	0.979	0.96
Adaptive neuro-fuzzy inference system (ANFIS)	3.3	0.959	0.92	3.6	0.964	0.91
Support vector regression (SVR)	5.3	0.916	0.84	6.3	0.916	0.84

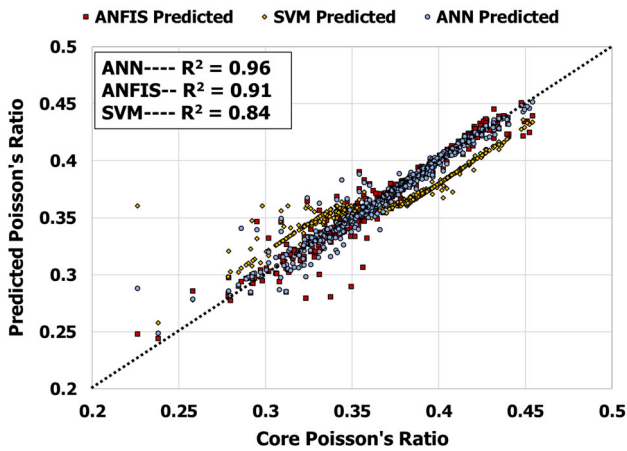


Fig. 9 Cross-plot comparison of the three different AI techniques on the overall data (training and testing)

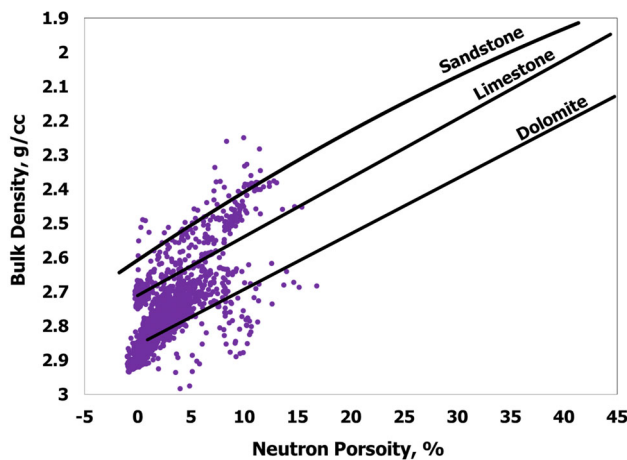


Fig. 10 Bulk density and neutron porosity lithology cross-plot of the well no. 1

Step 2 To apply Eq. (13), weights and biases are needed which are given in Table 4. The sequence of parameters that goes into the model is given as: bulk density, P-wave and S-wave transit times

Step 3 Equation (13) gives static Poisson’s ratio in normalized form in the range of [− 1 1]. It should be reversed back to original values by using Eq. (20).

$$\text{Output} = \frac{(y_{\max} - y_{\min})(\text{Output}_{\text{norm}} - (-1))}{1 - (-1)} + y_{\min} \quad (18)$$

y_{\max} and y_{\min} values (minimum and maximum values of static Poisson’s ratio) are given in Table 1. Therefore, Eq. (18) becomes

$$\text{PR}_{\text{Static}} = \frac{(0.475 - 0.167)(\text{PR}_{\text{static}_n} + 1)}{2} + 0.167 \quad (19)$$

$$\text{PR}_{\text{Static}} = 0.154 * \text{PR}_{\text{static}_n} + 0.321 \quad (20)$$

4.2 Validation

The newly proposed equation of ANN to predict static Poisson’s ratio is validated by three methods, namely, field validation, validation on published data, and validation by comparing the results with commonly used methods in the industry to predict static Poisson’s ratio.

4.2.1 Field validation

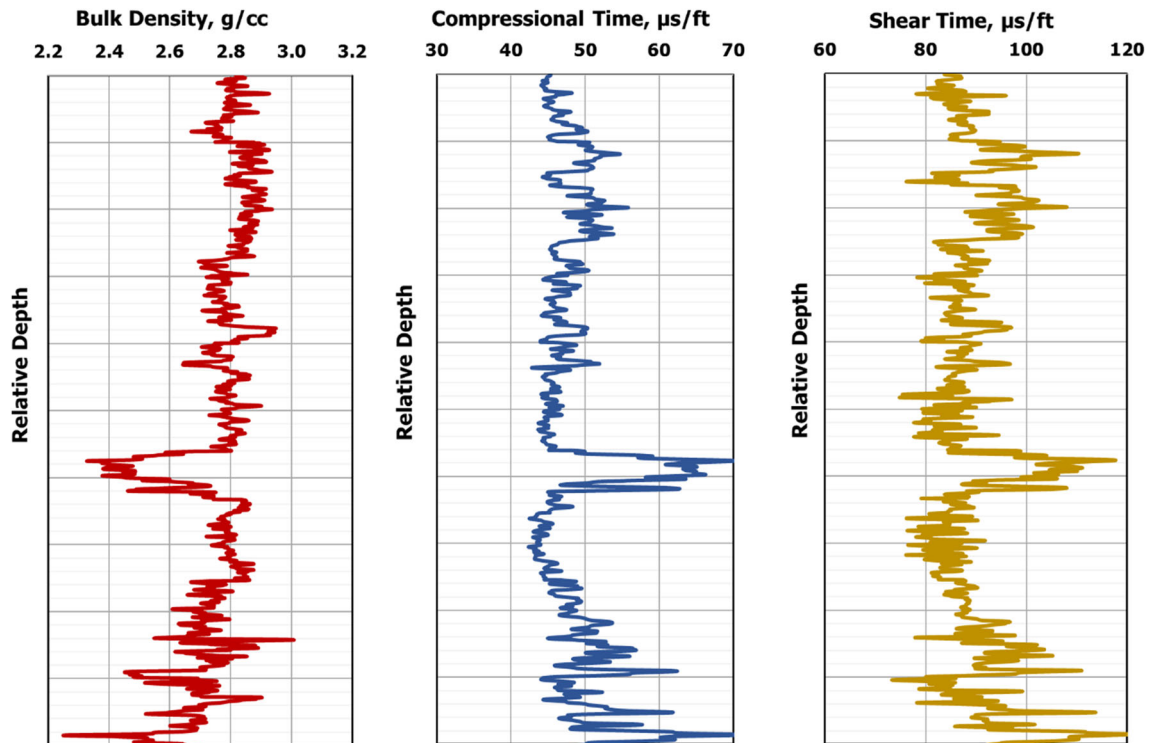
To validate the proposed model, the data from three separate wells were used. These data were not used in the training of the model.

Case 1

The input well log data consist of bulk density, P-wave transit time, and S-wave transit time. Laboratory data consist of measured static Poisson’s ratio using triaxial compressional tests. Lithology cross-plot of bulk density and neutron porosity is shown in Fig. 10 which depicts that most of the data in well no. 1 lie in limestone formation, with some percentage in dolomite and sandstone regions. Figure 11 shows the petrophysical well log data of well no. 1 for an interval of 1000 ft. The range of bulk density is in between 2.2 and 3.0 g/cc, the range of P-wave transit time is 40–70 μs/ft, and the range of S-wave transit time is 80–120 μs/ft. This well has thirteen core data points. The comparison of equation of ANN predicted and actual laboratory measured static Poisson’s ratio for well no. 1 is given in Fig. 12 which shows that equation of ANN predicted the static Poisson’s ratio for an interval of 1000 ft with R² of 0.9.

Table 4 Weights and biases of the new proposed equation of ANN

Hidden layer neurons (N_h)	Weights between input and hidden layer (w_1)			Weights between hidden and output layer (w_2)	Hidden layer biases (b_1)	Output layer bias (b_2)
	ρ	Δt_C	Δt_S			
1	1.4608	- 2.2688	2.3926	0.2646	- 4.1265	- 1.0122
2	2.9955	- 1.6475	0.3497	0.6757	- 4.2921	
3	1.7545	- 2.0612	- 2.0405	0.2994	- 3.2633	
4	2.9798	- 0.0147	2.4064	- 0.6677	- 1.6081	
5	1.9785	2.0895	- 2.3664	- 0.1202	- 2.3964	
6	0.2681	- 3.5618	- 1.0838	0.1861	- 1.7342	
7	- 1.2556	- 0.2136	- 3.6060	- 0.7493	- 1.0947	
8	- 3.4445	1.9341	0.7707	- 0.4598	1.1417	
9	1.5266	2.2339	- 1.9755	- 0.2148	- 0.2744	
10	- 2.7268	2.4850	- 1.5566	0.3788	0.5799	
11	- 2.0131	1.5304	2.6408	- 0.5060	- 0.9799	
12	- 3.4888	1.0297	1.9019	- 0.8081	- 0.9367	
13	- 2.7109	2.9644	0.3595	0.5450	- 0.8551	
14	- 2.7064	0.0478	- 0.0428	0.7256	- 1.0741	
15	2.4447	1.3262	2.5858	- 0.4331	1.4715	
16	- 0.7694	1.3039	- 3.3695	- 1.2325	- 1.5224	
17	- 0.6782	2.0970	1.2218	- 1.3940	- 3.9001	
18	0.5834	- 1.0022	- 3.3840	- 0.0178	- 2.3194	
19	2.1312	2.7246	- 1.1741	- 0.7072	3.5660	
20	- 1.2186	- 0.5271	- 3.6543	0.2265	- 3.6358	

**Fig. 11** A suite of petrophysical well log data for well no. 1. Track 1 represents bulk density log, track 2 represents P-wave transit time log, and track 3 represents S-wave transit time log

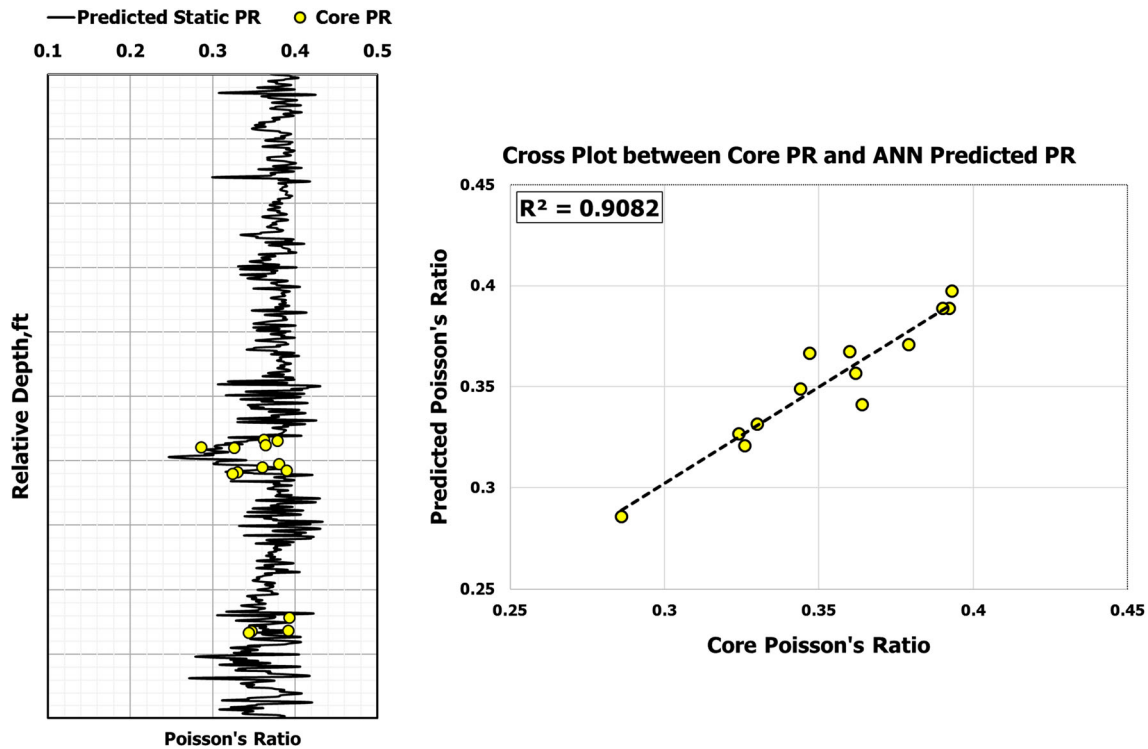


Fig. 12 Static Poisson's ratio prediction using proposed equation of ANN on well no. 1

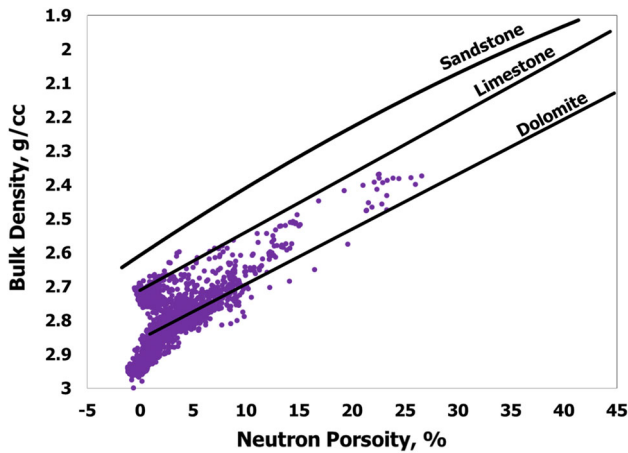


Fig. 13 Bulk density and neutron porosity lithology cross-plot of the well no. 2

Case 2

Well no. 2 lithology cross-plot between bulk density and neutron porosity is shown in Fig. 13 which indicates that most of the data lie in limestone formation, with some part in an anhydrite and dolomite regions. Anhydrites regions have zero porosity and density up to 3.0 g/cc. Input data of well no. 2 are given in Fig. 14. This well has five static Poisson's ratio values measured in the laboratory.

Figure 15 shows that equation of ANN predicted these five values with R^2 of 0.8.

Case 3

Well no. 3 lithology cross-plot between bulk density and neutron porosity is shown in Fig. 16 which indicates very scattered data, but majority of the data lie in the limestone formation, with some part in anhydrite and sandstone zones. Figure 17 shows the petrophysical well log input data for Well No. 3 for an interval of 400 ft. This well has four measured static Poisson's ratio values. Figure 18 shows the continuous profile of static Poisson's ratio for Well no. 3, including the accurate prediction of four laboratory measured static Poisson's ratio values with R^2 of 0.91.

4.2.2 Validation on published data

The new proposed equation of ANN is also tested on the published data by D'Andrea et al. [43]. In their work, 49 rock samples from different regions were tested for obtaining tensile strength, P-wave and S-wave velocities, Young's modulus, and Poisson's ratio. Figure 19 shows the input parameters, actual static Poisson's ratio, and predicted static Poisson's ratio values. From the analysis of Fig. 19, it is observed that new proposed equation of ANN can predict the static Poisson's ratio with AAPE of 6.5% and RMSE of 0.0228.

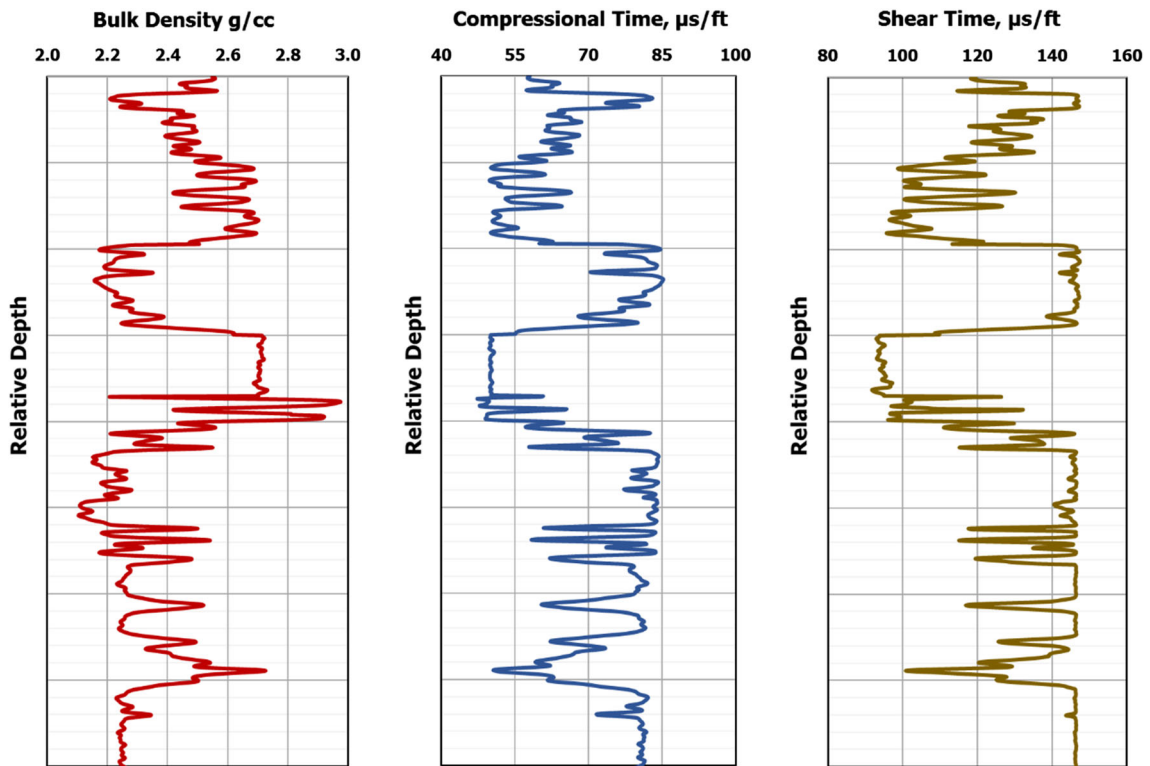


Fig. 14 A suite of petrophysical well log data for well no. 2. Track 1 represents bulk density log, track 2 represents P-wave transit time log, and track 3 represents S-wave transit time log

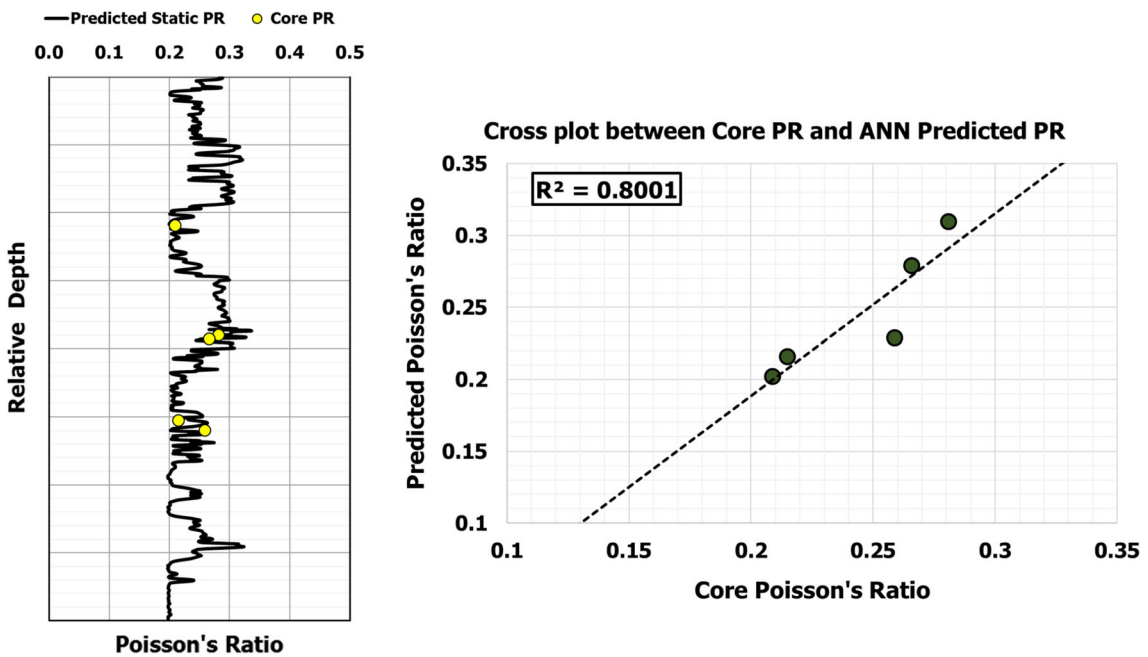


Fig. 15 Static Poisson's ratio prediction using proposed equation of ANN on well no. 2

4.2.3 Validation by comparison with common methods of estimating static Poisson’s ratio

It is customary in the petroleum industry to generate a continuous profile of the static Poisson’s ratio for the whole reservoir section by obtaining different correlations. These correlations are obtained by relating petrophysical well

logs such as neutron porosity, bulk density, P-wave transit time, and S-wave transit times with the laboratory measured values of the static Poisson’s ratio of the core samples. The core samples are obtained from the offset wells of the same field.

In this study, this approach of determining static Poisson’s ratio is tested against the results of the new proposed equation of ANN. Figure 20 shows the linear cross-plots of the static Poisson’s ratio with the dynamic Poisson’s ratio, bulk density, P-wave transit time, and S-wave transit time. Figure 20a shows the relationship between static Poisson’s ratio and dynamic Poisson’s ratio having R^2 of 0.026, Fig. 20b shows the linear relation between static Poisson’s ratio and bulk density with R^2 of 0.1, Fig. 20c shows the linear relation between static Poisson’s ratio and P-wave transit time with R^2 of 0.1, and Fig. 20d shows the relationship between static Poisson’s ratio and S-wave transit time with R^2 of 0.08.

Equations (21)–(24) are developed by correlating with these petrophysical well logs. These linear correlations were developed on the same dataset that was used for the training of the AI models.

$$PR_{Static} = 0.2416PR_{Dyn} + 0.2314 \tag{21}$$

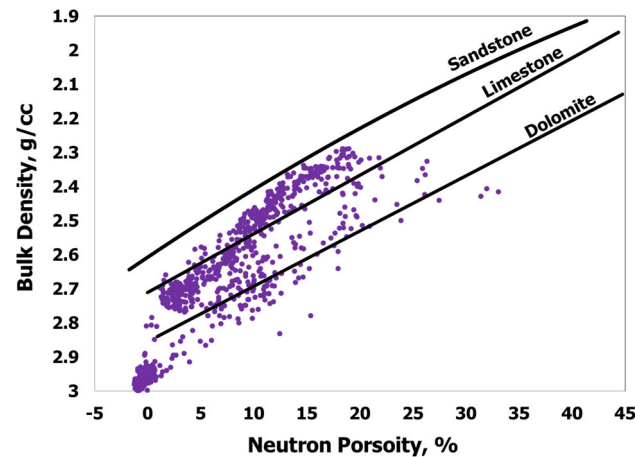


Fig. 16 Bulk density and neutron porosity lithology cross-plot of well no. 3

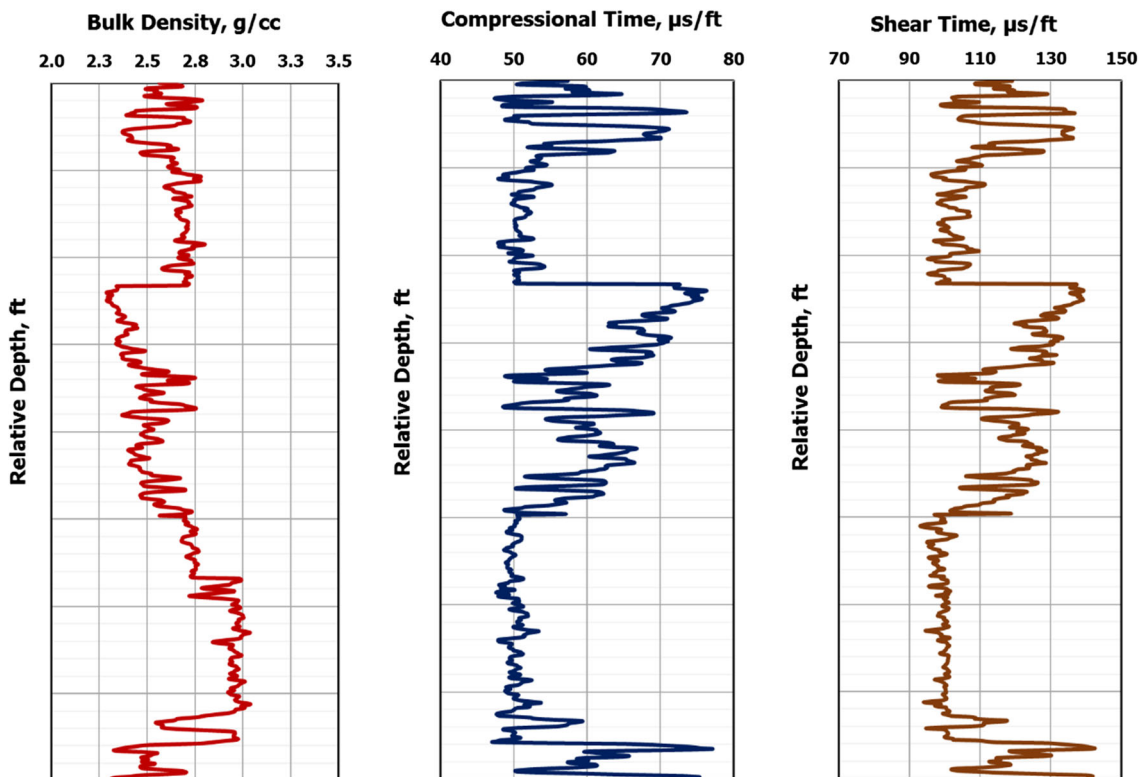


Fig. 17 A suite of petrophysical well log data for well no. 3. Track 1 represents bulk density log, track 2 represents P-wave transit time log, and track 3 represents S-wave transit time log

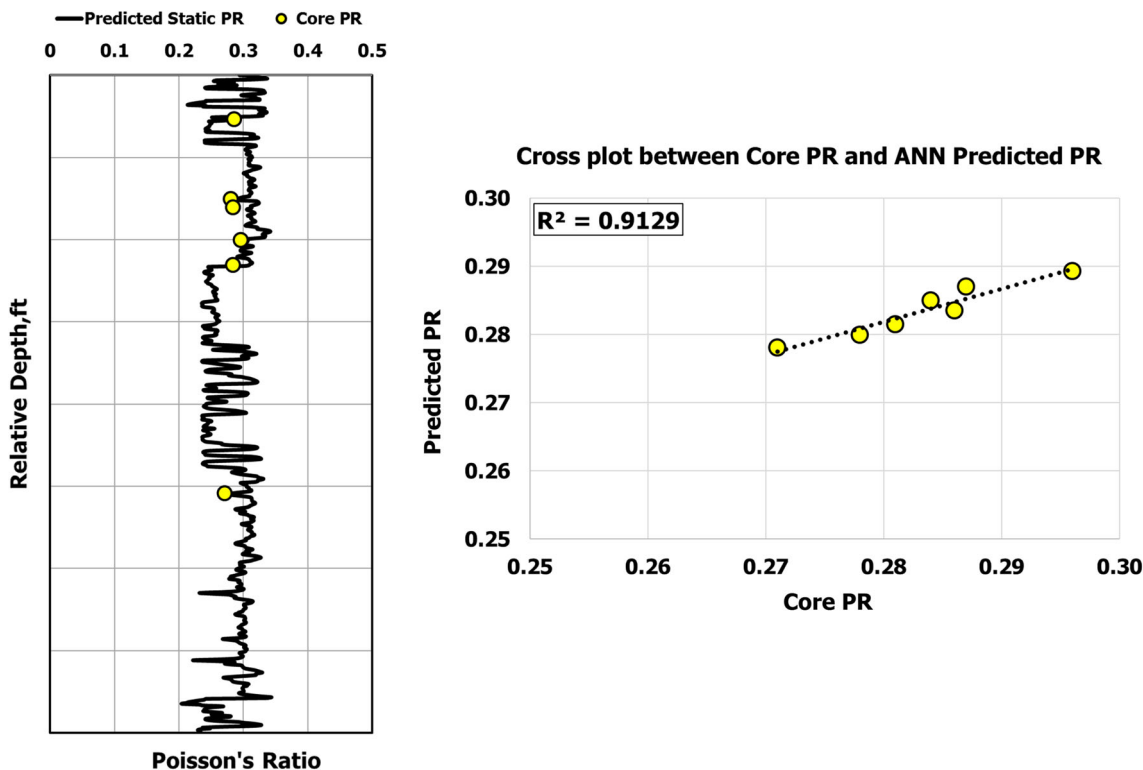


Fig. 18 Static Poisson's ratio prediction using proposed equation of ANN on Well No. 3

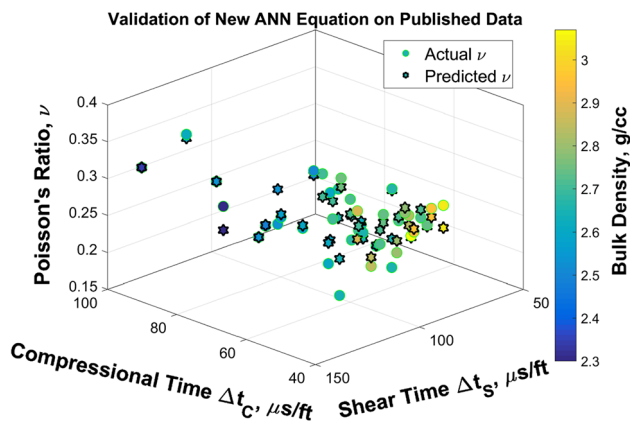


Fig. 19 Static Poisson's ratio prediction using proposed equation of ANN on published data by D'Andrea et al. [43]

$$PR_{Static} = 0.1686\rho + 0.1358 \tag{22}$$

$$PR_{Static} = 0.4526 - 0.0025\Delta t_C \tag{23}$$

$$PR_{Static} = 0.4523 - 0.0041\Delta t_S \tag{24}$$

The dynamic Poisson's ratio is calculated using Eq. 25.

$$PR_{dyn} = \frac{V_P^2 - 2V_S^2}{2(V_P^2 - V_S^2)} \tag{25}$$

V_P is the velocity of P-wave in km/s, and V_S is the velocity of S-wave in km/s.

Figure 21 shows continuous profiles of static Poisson's ratio obtained from Eqs. (21)–(24). The profiles generated from PR_{dyn} , P-wave transit time, and S-wave transit time show under-estimated values, while the profile generated from bulk density shows over-estimated values. From these correlations, the static Poisson's ratio profiles generated did not match with any laboratory determined static Poisson's ratio values, while the new proposed equation of ANN matched with almost every actual data point. Figure 21 shows the AAPE bar chart for each correlation, demonstrating the high accuracy of proposed equation of ANN.

5 Conclusions and recommendations

The predictive efficiency of AI techniques (ANN, ANFIS, and SVR) to model static Poisson's ratio is investigated in this study. The results reveal that

1. ANN performed better than ANFIS and SVR by giving less AAPE and high R^2 .
2. By the development of equation of ANN, the black box nature of an ANN is converted into a white box by obtaining tangible weights and biases from the trained ANN model.
3. Equation of ANN can predict the static Poisson's ratio using three commonly available petrophysical well

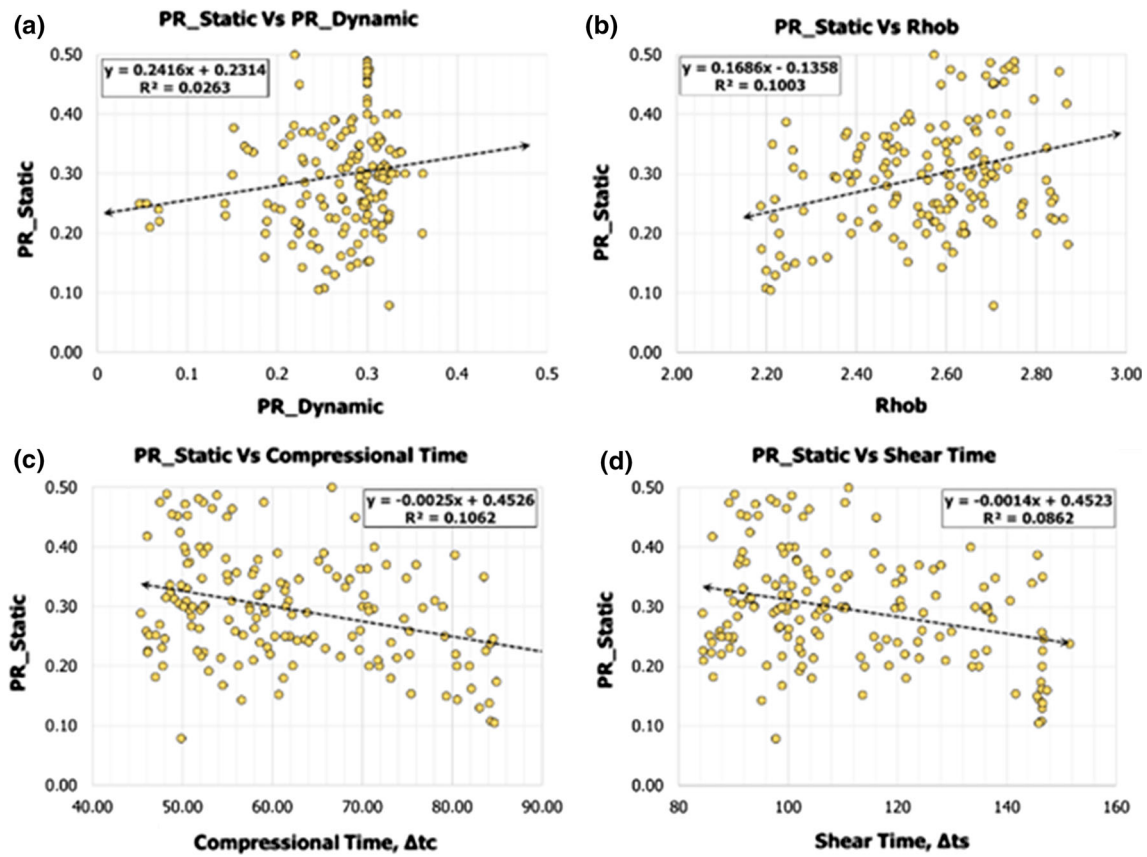


Fig. 20 Linear relation of static Poisson’s ratio with petrophysical well logs. **a** Relationship between static Poisson’s ratio and dynamic Poisson’s ratio. **b** Relationship between static Poisson’s ratio and bulk

density. **c** Relationship between static Poisson’s ratio and P-wave transit time. **d** Relationship between static Poisson’s ratio and S-wave transit time

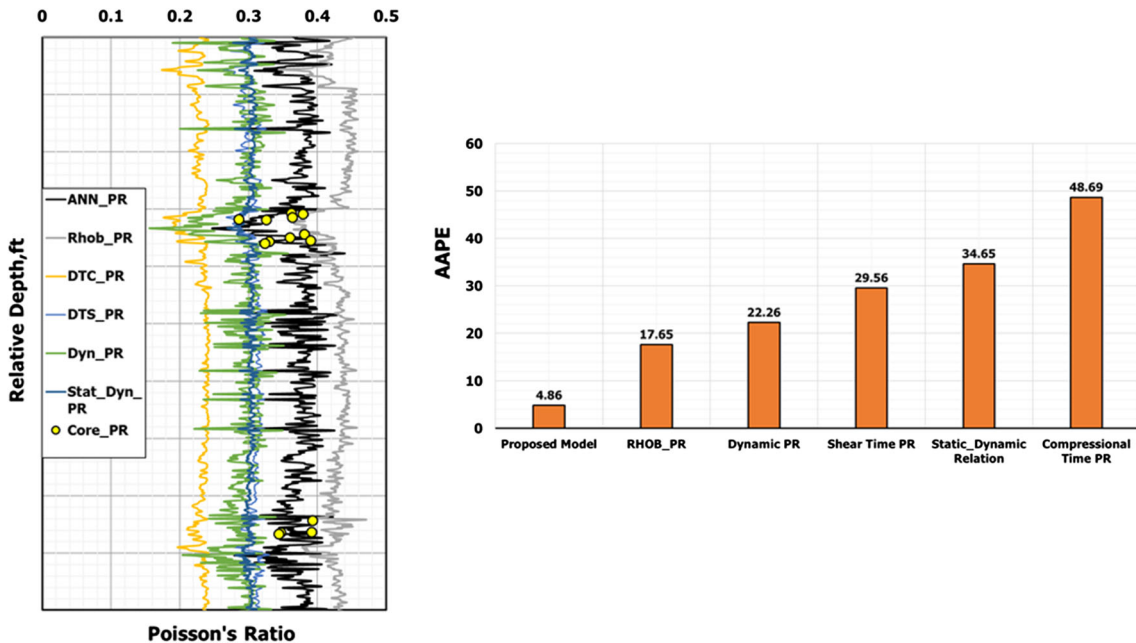


Fig. 21 Validation comparison of new equation of ANN against linear correlations (Eqs. 21–24) to predict static Poisson’s ratio

logs namely, bulk density, P-wave, and S-wave transit times

4. Equation of ANN provides better static Poisson's ratio estimations compared to available methods as shown by lower AAPE and higher R^2 .
5. Equation of ANN can be used in wells with no static Poisson's ratio data or the wells with cased hole, where estimation of the static Poisson's ratio is not possible.
6. The new equation of ANN can be used for the prediction in new wells without the need of any AI software.
7. The new equation can give the real-time values of static Poisson's ratio of carbonate rocks wherever the real-time logs are available.
8. From overall results produced, it can be said that AI techniques can be used as a cost-effective alternative in terms of saving the number of experiments to calculate static Poisson's ratio.

In this study, the core samples tested were in dry condition and the equation of ANN developed is valid for dry conditions. It is recommended to conduct the same testing under saturated condition and observe the difference of static Poisson's ratio values in both dry and saturated conditions, and the model performance in saturated conditions. Also, more AI techniques can be explored such as decision trees, type 2 fuzzy logic, and functional networks.

Acknowledgements The authors would like to acknowledge College of Petroleum & Geosciences (CPG), King Fahd University of Petroleum & Minerals for providing research opportunities to produce this paper.

Compliance with ethical standards

Conflict of interest The authors declare that they have no conflict of interest.

Appendix A

Average absolute percentage error (AAPE) is defined as follows:

$$AAPE = \frac{\sum \left| (PR_{static_{measured}} - PR_{static_{predicted}}) \right|}{k} * \frac{100}{PR_{static_{measured}}} \quad (26)$$

Root mean square error (RMSE) is defined as follows:

$$RMSE = \sqrt{\frac{\sum (PR_{static_{measured}} - PR_{static_{predicted}})^2}{k}} \quad (27)$$

where $PR_{static_{measured}}$ is the measured value of PR_{static} and $PR_{static_{predicted}}$ is the estimated value from the models. k is the total number of data points.

Pearson correlation coefficient CC is defined as follows:

$$CC = \frac{k \sum xy - (\sum x)(\sum y)}{\sqrt{k(\sum x^2) - (\sum y)^2} \sqrt{k(\sum b^2) - (\sum b)^2}} \quad (28)$$

where x and y are two variables.

Coefficient of determination R^2 is defined as follows:

$$R^2 = \left(\frac{k \sum xy - (\sum x)(\sum y)}{\sqrt{k(\sum x^2) - (\sum y)^2} \sqrt{k(\sum b^2) - (\sum b)^2}} \right)^2 \quad (29)$$

References

1. Anifowose F, Labadin J, Abdurraheem A (2015) Improving the prediction of petroleum reservoir characterization with a stacked generalization ensemble model of support vector machines. *Appl Soft Comput* 26:483–496. <https://doi.org/10.1016/j.asoc.2014.10.017>
2. Anifowose F, Adeniyi S, Abdurraheem A, Al-Shuhail A (2016) Integrating seismic and log data for improved petroleum reservoir properties estimation using non-linear feature-selection based hybrid computational intelligence models. *J Pet Sci Eng* 145:230–237. <https://doi.org/10.1016/j.petrol.2016.05.019>
3. Anifowose FA, Labadin J, Abdurraheem A (2015) Ensemble model of non-linear feature selection-based extreme learning machine for improved natural gas reservoir characterization. *J Nat Gas Sci Eng* 26:1561–1572. <https://doi.org/10.1016/j.jngse.2015.02.012>
4. Anifowose FA, Labadin J, Abdurraheem A (2017) Ensemble machine learning: an untapped modeling paradigm for petroleum reservoir characterization. *J Pet Sci Eng* 151:480–487. <https://doi.org/10.1016/j.petrol.2017.01.024>
5. Helmy T, Hossain MI, Abdurraheem A et al (2017) Prediction of non-hydrocarbon gas components in separator by using hybrid computational intelligence models. *Neural Comput Appl* 28:635–649. <https://doi.org/10.1007/s00521-015-2088-4>
6. Al-Bulushi NI, King PR, Blunt MJ, Kraaijveld M (2012) Artificial neural networks workflow and its application in the petroleum industry. *Neural Comput Appl* 21:409–421. <https://doi.org/10.1007/s00521-010-0501-6>
7. Mohaghegh S (1995) Neural network: what it can do for petroleum engineers. *J Pet Technol* 47:42. <https://doi.org/10.2118/29219-PA>
8. Elkatatny S, Mahmoud M, Tariq Z, Abdurraheem A (2017) New insights into the prediction of heterogeneous carbonate reservoir permeability from well logs using artificial intelligence network. *Neural Comput Appl*. <https://doi.org/10.1007/s00521-017-2850-x>
9. Tariq Z, Elkatatny S, Mahmoud M, Abdurraheem A (2016) A new artificial intelligence based empirical correlation to predict sonic travel time. In: International petroleum technology conference. International Petroleum Technology Conference
10. Najibi AR, Ghafoori M, Lashkaripour GR, Asef MR (2015) Empirical relations between strength and static and dynamic elastic properties of Asmari and Sarvak limestones, two main oil reservoirs in Iran. *J Pet Sci Eng* 126:78–82. <https://doi.org/10.1016/j.petrol.2014.12.010>

11. Abdurraheem A, Sabakhy E, Ahmed M et al (2007) Estimation of permeability from wireline logs in a middle eastern carbonate reservoir using fuzzy logic. In: SPE middle east oil and gas show and conference. Society of Petroleum Engineers
12. Nooruddin HA, Anifowose F, Abdurraheem A (2013) Applying artificial intelligence techniques to develop permeability predictive models using mercury injection capillary-pressure data. In: SPE Saudi Arabia section technical symposium and exhibition. Society of Petroleum Engineers
13. Anifowose F, Labadin J, Abdurraheem A (2013) A least-square-driven functional networks type-2 fuzzy logic hybrid model for efficient petroleum reservoir properties prediction. *Neural Comput Appl* 23:179–190. <https://doi.org/10.1007/s00521-012-1298-2>
14. Helmy T, Rahman SM, Hossain MI, Abdurraheem A (2013) Non-linear heterogeneous ensemble model for permeability prediction of oil reservoirs. *Arab J Sci Eng* 38:1379–1395. <https://doi.org/10.1007/s13369-013-0588-z>
15. Shujath Ali S, Hossain ME, Hassan MR, Abdurraheem A (2013) Hydraulic unit estimation from predicted permeability and porosity using artificial intelligence techniques. In: North Africa technical conference and exhibition. Society of Petroleum Engineers
16. Abdurraheem A, Ahmed M, Vantala A, Parvez T (2009) Prediction of rock mechanical parameters for hydrocarbon reservoirs using different artificial intelligence techniques. In: SPE Saudi Arabia section Technical Symposium. Society of Petroleum Engineers
17. Tariq Z, Elkatatny S, Mahmoud M, Abdurraheem A (2016) A holistic approach to develop new rigorous empirical correlation for static Young's Modulus. In: Abu Dhabi international petroleum exhibition & conference. Society of Petroleum Engineers
18. Tariq Z, Elkatatny S, Mahmoud M et al (2017) A new approach to predict failure parameters of carbonate rocks using artificial intelligence tools. In: SPE Kingdom of Saudi Arabia annual technical symposium and exhibition. Society of Petroleum Engineers
19. Tariq Z, Elkatatny S, Mahmoud M et al (2017) A new technique to develop rock strength correlation using artificial intelligence tools. In: SPE reservoir characterisation and simulation conference and exhibition. Society of Petroleum Engineers
20. Yang Y, Rosenbaum MS (2002) The artificial neural network as a tool for assessing geotechnical properties. *Geotech Geol Eng* 20:149–168. <https://doi.org/10.1023/A:1015066903985>
21. Sonmez H, Tuncay E, Gokceoglu C (2004) Models to predict the uniaxial compressive strength and the modulus of elasticity for Ankara agglomerate. *Int J Rock Mech Min Sci* 41:717–729. <https://doi.org/10.1016/j.ijrmms.2004.01.011>
22. Cevik A, Sezer EA, Cabalar AF, Gokceoglu C (2011) Modeling of the uniaxial compressive strength of some clay-bearing rocks using neural network. *Appl Soft Comput* 11:2587–2594. <https://doi.org/10.1016/j.asoc.2010.10.008>
23. Elkatatny S, Tariq Z, Mahmoud M et al (2018) Development of new mathematical model for compressional and shear sonic times from wireline log data using artificial intelligence neural networks (white box). *Arab J Sci Eng*. <https://doi.org/10.1007/s13369-018-3094-5>
24. Bazargan H, Adibifard M (2017) A stochastic well-test analysis on transient pressure data using iterative ensemble Kalman filter. *Neural Comput Appl*. <https://doi.org/10.1007/s00521-017-3264-5>
25. Artun E (2017) Characterizing interwell connectivity in water-flooded reservoirs using data-driven and reduced-physics models: a comparative study. *Neural Comput Appl* 28:1729–1743. <https://doi.org/10.1007/s00521-015-2152-0>
26. Fattahi H, Gholami A, Amiribakhtiar MS, Moradi S (2015) Estimation of asphaltene precipitation from titration data: a hybrid support vector regression with harmony search. *Neural Comput Appl* 26:789–798. <https://doi.org/10.1007/s00521-014-1766-y>
27. Alimohammadi S, Sayyad Amin J, Nikoee E (2017) Estimation of asphaltene precipitation in light, medium and heavy oils: experimental study and neural network modeling. *Neural Comput Appl* 28:679–694. <https://doi.org/10.1007/s00521-015-2097-3>
28. Adebayo AR, Abdurraheem A, Olatunji SO (2015) Artificial intelligence based estimation of water saturation in complex reservoir systems. *J Porous Media* 18:893–906. <https://doi.org/10.1615/JPorMedia.v18.i9.60>
29. Baziari S, Shahripour HB, Tadayoni M, Nabi-Bidhendi M (2016) Prediction of water saturation in a tight gas sandstone reservoir by using four intelligent methods: a comparative study. *Neural Comput Appl*. 10:15–20. <https://doi.org/10.1007/s00521-016-2729-2>
30. Gatens JM, Harrison CW, Lancaster DE, Guidry FK (1990) In-situ stress tests and acoustic logs determine mechanical properties and stress profiles in the devonian shales. *SPE Form Eval* 5:248–254. <https://doi.org/10.2118/18523-PA>
31. Chang C, Zoback MD, Khaksar A (2006) Empirical relations between rock strength and physical properties in sedimentary rocks. *J Pet Sci Eng* 51:223–237. <https://doi.org/10.1016/j.petrol.2006.01.003>
32. Khaksar A, Taylor PG, Fang Z et al (2009) Rock strength from core and logs, where we stand and ways to go. In: EUROPEC/EAGE conference and exhibition. Society of Petroleum Engineers
33. Nes O-M, Fjær E, Tronvoll J et al (2005) Drilling time reduction through an integrated rock mechanics analysis. In: SPE/IADC drilling conference. Society of Petroleum Engineers
34. Chan T, Hood M, Board M (1982) Rock properties and their effect on thermally induced displacements and stresses. *J Energy Resour Technol* 104:384. <https://doi.org/10.1115/1.3230433>
35. Cadwallader S, Wampler J, Sun T et al (2015) An integrated dataset centered around distributed fiber optic monitoring—key to the successful implementation of a geo-engineered completion optimization program in the eagle ford shale. In: Proceedings of the 3rd unconventional resources technology conference. American Association of Petroleum Geologists, Tulsa, OK, USA
36. Wang C, Wu Y-S, Xiong Y et al (2015) Geomechanics coupling simulation of fracture closure and its influence on gas production in shale gas reservoirs. In: SPE reservoir simulation symposium. Society of Petroleum Engineers
37. Nawrocki PA, Dusseault MB (1996) Modelling of damaged zones around boreholes using a radius dependent Young's modulus. *J Can Pet Technol*. <https://doi.org/10.2118/96-03-04>
38. Ameen MS, Smart BGD, Somerville JM et al (2009) Predicting rock mechanical properties of carbonates from wireline logs (a case study: arab-D reservoir, Ghawar field, Saudi Arabia). *Mar Pet Geol* 26:430–444. <https://doi.org/10.1016/j.marpetgeo.2009.01.017>
39. Elkatatny S, Tariq Z, Mahmoud M et al (2018) An integrated approach for estimating static Young's modulus using artificial intelligence tools. *Neural Comput Appl*. <https://doi.org/10.1007/s00521-018-3344-1>
40. Tariq Z, Elkatatny SM, Mahmoud MA, Abdurraheem A, Abdelwahab AZ, Woldeamanuel M (2017) Estimation of rock mechanical parameters using artificial intelligence tools. American Rock Mechanics Association
41. Mahmoud M, Elkatatny S, Ramadan E, Abdurraheem A (2016) Development of lithology-based static Young's modulus correlations from log data based on data clustering technique. *J Pet Sci Eng* 146:10–20. <https://doi.org/10.1016/j.petrol.2016.04.011>
42. Tariq Z, Elkatatny SM, Mahmoud MA et al (2017) Development of new correlation of unconfined compressive strength for carbonate reservoir using artificial intelligence techniques. In: 51st US rock mechanics/geomechanics symposium 2017

43. D'Andrea D V., Fischer RL, Fogelson DE (1965) Prediction of compressive strength from other rock properties. United States Department of The Interior Bureau of Mines
44. Kumar A, Jayakumar T, Raj B, Ray KK (2003) Correlation between ultrasonic shear wave velocity and Poisson's ratio for isotropic solid materials. *Acta Mater* 51:2417–2426. [https://doi.org/10.1016/S1359-6454\(03\)00054-5](https://doi.org/10.1016/S1359-6454(03)00054-5)
45. Phani KK (2008) Correlation between ultrasonic shear wave velocity and Poisson's ratio for isotropic porous materials. *J Mater Sci* 43:316–323. <https://doi.org/10.1007/s10853-007-2055-2>
46. Edimann K, Somerville JM, Smart BGD et al (1998) Predicting rock mechanical properties from wireline porosities. In: SPE/ISRM rock mechanics in petroleum engineering. Society of Petroleum Engineers
47. Al-Shayea NA (2004) Effects of testing methods and conditions on the elastic properties of limestone rock. *Eng Geol* 74:139–156. <https://doi.org/10.1016/j.enggeo.2004.03.007>
48. Singh V, Singh TN (2006) A neuro-fuzzy approach for prediction of Poisson's ratio and young's modulus of shale and sandstone. In: The 41st U.S. symposium on rock mechanics (USRMS), 17–21 June, Golden, Colorado
49. Shalabi FI, Cording EJ, Al-Hattamleh OH (2007) Estimation of rock engineering properties using hardness tests. *Eng Geol* 90:138–147. <https://doi.org/10.1016/j.enggeo.2006.12.006>
50. Al-Anazi A, Gates ID (2010) A support vector machine algorithm to classify lithofacies and model permeability in heterogeneous reservoirs. *Eng Geol* 114:267–277. <https://doi.org/10.1016/j.enggeo.2010.05.005>
51. Baykasoğlu A, Dereli T, Tanış S (2004) Prediction of cement strength using soft computing techniques. *Cem Concr Res* 34:2083–2090. <https://doi.org/10.1016/j.cemconres.2004.03.028>
52. ASTM D-04 (2005) Standard test method for triaxial compressive strength of undrained rock core specimens without pore pressure measurements
53. Rao S, Ramamurti V (1993) A hybrid technique to enhance the performance of recurrent neural networks for time series prediction. In: IEEE international conference on neural networks. IEEE, pp 52–57
54. Angelini E, Ludovici A (2009) CDS Evaluation model with neural networks. *J Serv Sci Manag* 02:15–28. <https://doi.org/10.4236/jssm.2009.21003>
55. Monjezi M, Dehghani H (2008) Evaluation of effect of blasting pattern parameters on back break using neural networks. *Int J Rock Mech Min Sci* 45:1446–1453. <https://doi.org/10.1016/j.ijrmm.2008.02.007>
56. Hinton GE, Osindero S, Teh Y-W (2006) A Fast Learning Algorithm For Deep Belief Nets. *Neural Comput* 18:1527–1554. <https://doi.org/10.1162/neco.2006.18.7.1527>
57. Lippmann R (1994) Book review: "Neural Networks, A Comprehensive Foundation", by Simon Haykin. *Int J Neural Syst* 05:363–364. <https://doi.org/10.1142/S0129065794000372>
58. Vineis P, Rainoldi A (1997) Neural networks and logistic regression: analysis of a case-control study on myocardial infarction. *J Clin Epidemiol* 50:1309–1310. [https://doi.org/10.1016/S0895-4356\(97\)00163-7](https://doi.org/10.1016/S0895-4356(97)00163-7)
59. Yilmaz I, Yuksek AG (2008) An example of artificial neural network (ANN) application for indirect estimation of rock parameters. *Rock Mech Rock Eng* 41:781–795. <https://doi.org/10.1007/s00603-007-0138-7>
60. Yagiz S, Sezer EA, Gokceoglu C (2012) Artificial neural networks and nonlinear regression techniques to assess the influence of slake durability cycles on the prediction of uniaxial compressive strength and modulus of elasticity for carbonate rocks. *Int J Numer Anal Methods Geomech* 36:1636–1650. <https://doi.org/10.1002/nag.1066>
61. Mohaghegh SD (2017) *Shale Analytics*. Springer, Cham
62. Jang J-SR (1993) ANFIS: adaptive-network-based fuzzy inference system. *IEEE Trans Syst Man Cybern* 23:665–685. <https://doi.org/10.1109/21.256541>
63. Jang J-SR (1996) Input selection for ANFIS learning. In: Proceedings of IEEE 5th international fuzzy systems. IEEE, pp 1493–1499
64. Jang J-SR, Sun Chuen-Tsai (1995) Neuro-fuzzy modeling and control. *Proc IEEE* 83:378–406. <https://doi.org/10.1109/5.364486>
65. Ebrahimi M, Sajedian A (2010) Use of fuzzy logic for predicting two phase inflow performance relationship of horizontal oil wells. In: Trinidad and tobago energy resources conference. Society of Petroleum Engineers
66. Walia N, Singh H, Sharma A (2015) ANFIS: adaptive neuro-fuzzy inference system—a survey. *Int J Comput Appl* 123:32–38. <https://doi.org/10.5120/ijca2015905635>
67. Tahmasebi P, Hezarkhani A (2012) A hybrid neural networks-fuzzy logic-genetic algorithm for grade estimation. *Comput Geosci* 42:18–27. <https://doi.org/10.1016/j.cageo.2012.02.004>
68. El-Sebakhy EA, Hadi AS, Faisal KA (2007) Iterative least squares functional networks classifier. *IEEE Trans Neural Networks* 18:844–850. <https://doi.org/10.1109/TNN.2007.891632>
69. Elhaj MA, Anifowose F, Abdurraheem A, Fahad K (2015) Single gas flow prediction through chokes using artificial intelligence techniques. SPE Saudi Arabia Section Annual Technical Symposium and Exhibition, 21–23 April, Al-Khobar, Saudi Arabia. <https://doi.org/10.2118/177991-MS>
70. Anifowose F, Adeniye S, Abdurraheem A (2014) Recent advances in the application of computational intelligence techniques in oil and gas reservoir characterisation: a comparative study. *J Exp Theor Artif Intell* 26:551–570. <https://doi.org/10.1080/0952813X.2014.924577>
71. Trontl K, Šmuc T, Pevec D (2007) Support vector regression model for the estimation of γ -ray buildup factors for multi-layer shields. *Ann Nucl Energy* 34:939–952. <https://doi.org/10.1016/j.anucene.2007.05.001>
72. Jeng J-T, Chuang C-C, Su S-F (2003) Support vector interval regression networks for interval regression analysis. *Fuzzy Sets Syst* 138:283–300. [https://doi.org/10.1016/S0165-0114\(02\)00570-5](https://doi.org/10.1016/S0165-0114(02)00570-5)
73. Khoukhi A, Oloso M, Elshafei M et al (2011) Support vector regression and functional networks for viscosity and gas/oil ratio curves estimation. *Int J Comput Intell Appl* 10:269–293. <https://doi.org/10.1142/S1469026811003100>
74. Guo G (2014) *Support vector machines applications*. Springer, Cham
75. Eberhart R, Kennedy J (1995) A new optimizer using particle swarm theory. In: MHS'95. Proceedings of the sixth international symposium on micro machine and human science. IEEE, pp 39–43
76. Kennedy J (1997) The particle swarm: social adaptation of knowledge. In: Proceedings of 1997 IEEE international conference on evolutionary computation (ICEC'97). IEEE, pp 303–308
77. Tariq Z, Abdurraheem A, Khan MR, Sadeed A (2018) New inflow performance relationship for a horizontal well in a naturally fractured solution gas drive reservoirs using artificial intelligence technique. In: Offshore technology conference Asia. Offshore Technology Conference
78. Eberhart RC, Shi Y (1998) Comparison between genetic algorithms and particle swarm optimization. In: International conference on evolutionary programming, pp 611–616
79. Hagan MT, Menhaj MB (1994) Training feedforward networks with the Marquardt algorithm. *IEEE Trans Neural Networks* 5:989–993. <https://doi.org/10.1109/72.329697>
80. Bello O, Asafa T (2014) A functional networks softsensor for flowing bottomhole pressures and temperatures in multiphase

- production wells. In: SPE intelligent energy conference & exhibition. Society of Petroleum Engineers
81. Awadalla M, Yousef H (2016) Neural networks for flow bottom hole pressure prediction. *Int J Electr Comput Eng* 6:1839. <https://doi.org/10.11591/ijece.v6i4.10774>
82. Memon PQ, Yong S-P, Pao W, Sean PJ (2014) Surrogate reservoir modeling-prediction of bottom-hole flowing pressure using radial basis neural network. In: 2014 Science and information conference. IEEE, pp 499–504
83. Jahanandish I, Salimifard B, Jalalifar H (2011) Predicting bottomhole pressure in vertical multiphase flowing wells using artificial neural networks. *J Pet Sci Eng* 75:336–342. <https://doi.org/10.1016/j.petrol.2010.11.019>
84. Osman E-SA, Ayoub MA, Aggour MA (2005) An artificial neural network model for predicting bottomhole flowing pressure in vertical multiphase flow. In: SPE middle east oil and gas show and conference. Society of Petroleum Engineers
85. Ebrahimi A, Khamehchi E (2015) A robust model for computing pressure drop in vertical multiphase flow. *J Nat Gas Sci Eng* 26:1306–1316. <https://doi.org/10.1016/j.jngse.2015.08.036>
86. Adebayo AR, Abdulraheem A, Al-Shammari AT (2013) Promises of artificial intelligence techniques in reducing errors in complex flow and pressure losses calculations in multiphase fluid flow in oil wells. In: SPE Nigeria annual international conference and exhibition. Society of Petroleum Engineers

Publisher's Note Springer Nature remains neutral with regard to jurisdictional claims in published maps and institutional affiliations.